Available online at www.sciencedirect.com
SCIENCE DIRECT®
Coordination Chemistry Reviews 248 (2004) 817–834
COORDINATION CHEMISTRY REVIEWS
www.elsevier.com/locate/ccr

Review

Metal phosphanido and metal arsanido cage compounds of aluminium, gallium and indium

Bernhard Neumüller*, Effat Iravani

Fachbereich Chemie der Universität Marburg, Hans-Meerwein-Strasse, D-35032 Marburg, Germany

Received 20 August 2003; accepted 20 April 2004

Contents

Abstract

This article presents a comparison of phosphanido and arsanido complexes of the metals aluminium, gallium and indium with cage structure. The synthesis and the structures have been discussed especially with respect to the structures of ME (M = Al, Ga, In; E = P, As).

Keywords: Metal phosphanides; Metal arsanides; Group 13

1. Introduction

Compounds with the element combination group 13 (M)/group 15 (E = P, As) became interesting during the last 15 years for a couple of reasons [1]. On the one hand, there was a lack of information concerning the synthesis and the structures of such compounds in particular in the build-up of large M–E cage molecules [2]. On the other hand, one of the driving forces was the search for new single source precursors containing M–E bonds for generating thin layers of the corresponding materials ME. A series of review articles dealt with this subject [3–7] including the related nitrides.

A topic of continuous interest is the π-electron participation in M–E bonds by back-donation of the P or As lone pair into the formally empty p-orbitals of the metal atom [5,6]. Usually this contribution in addition to the σ-bond is not very high, even in Al–N bonds [8]. Very recently, an example of a Ga–As compound possessing Ga–As bonds with multiple bond character was published [9]. However, the normal way for interaction of the lone pair at E and the Lewis acid M is the formation of rings and cages [2]. A variety of structural motifs are posssible for the generation of M–E cages (Scheme 1) mostly containing M–E four-membered rings as in heterocubanes and heteroprismanes (six-membered ring as basal plane). Other cages such as heteroadamantanes or rhombic dodecahedrons can be found when the M:E ratio is 6:4 or when a third element is part of the cage skeleton.

Interestingly, two basic structures known from solid state chemistry can be used as archetypes to derive some of the cage architectures or at least a part of those. All structural motifs which contain a hexagonal heteroprismane are based on the Wurtzite lattice and the adamantane-like cages are based on the Zinc Blende lattice (Scheme 1). The thermo-

* Corresponding author. Tel.: +49 6421 28 22406; fax: +49 6421 28 25653.
E-mail address: neumuell@chemie.uni-marburg.de (B. Neumüller).

0010-8545/$ – see front matter © 2004 Elsevier B.V. All rights reserved.
doi:10.1016/j.ccr.2004.04.010

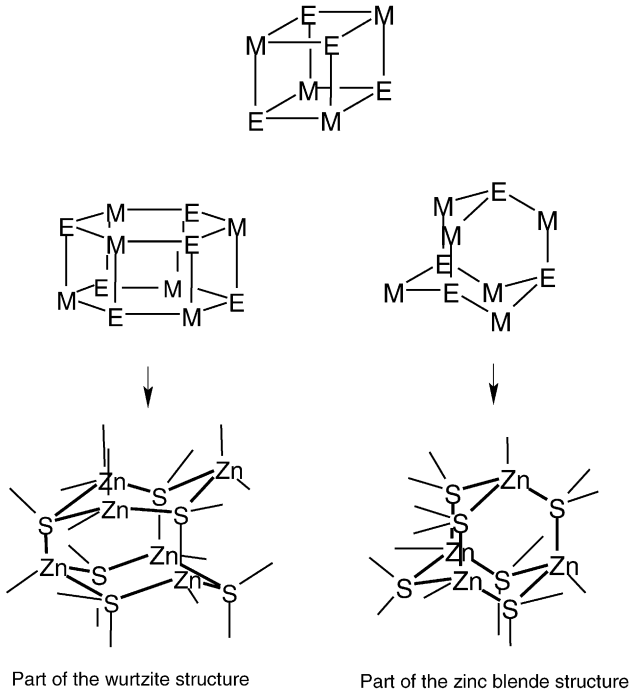

Scheme 1. Heteroprismane and heteroadamantane structures derived from the Wurtzite and the Zinc Blende structure.

dynamically stable structure type of GaE (P, As) and InE at room temperature is the Zinc Blende [10].

2. Aluminium compounds

There are a principally two ways to synthesize M–E cage structure compounds. The first one is the elimination of H_2 by reacting compounds with Al–H and H–E bonds. The second route is based on salt metathesis when metal halide functions where treated with M′–E functions (M′ = alkali metal). Depending on the electronical and steric behaviour of the sustituents on M and E all types of cages mentioned above could be realized. The heterocubane molecules are simple representatives first structurally characterized in 1990 Eq. (1). Example **1** is the only one reported in aluminium chemistry to date [11].

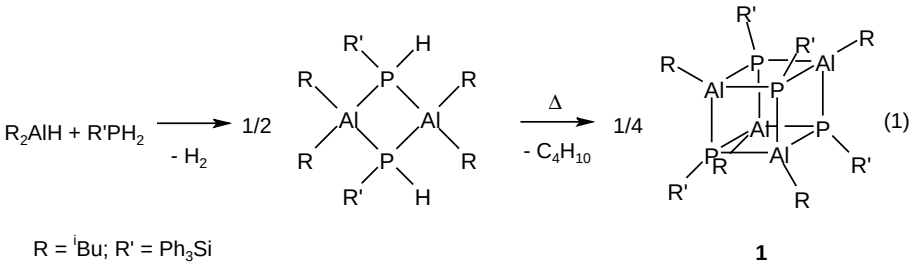

(1)

A lower steric demand by the substituents usually leads to a larger ring. This was realized with donor-stabilized aluminium hydride $[AlH_3(NMe_3)]$ and silicon substituted phosphanes and arsanes [12]. An alternative is the metathesis reaction of $AlCl_3$ with a dilithiated phosphane giving **2e** [13]. Two six-membered rings dimerize formally to the heteroprismanes **2a–e** Eq. (2).

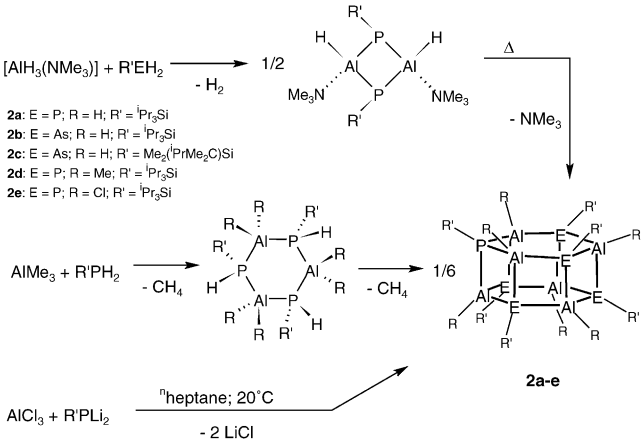

(2)

A heptameric Al–P skeleton in $(RAlPR')_7$ (**3**) (R = H; R′ = $SiMe_2(CMe_2^iPr)$) is one of the results in the reaction of $[AlH_3(NMe_3)]$ with H_2PR' Eq. (3) [14].

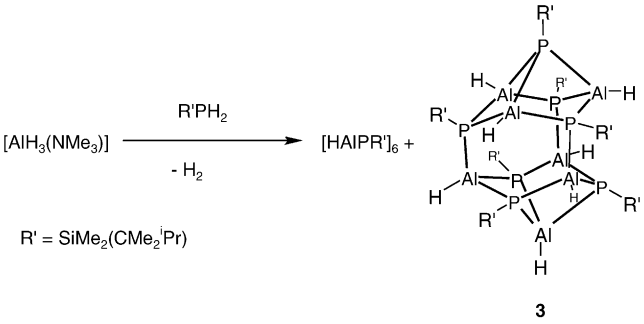

(3)

The third element in Al cage compounds is very often lithium. Li^+ ions are bound to the element of group 15 but also to the substituents on E, especially when hydrogen is a substituent. **4** was generated in the subsequent reaction of $^iPr_3SiPH_2$ with ^{n}BuLi and Me_2AlCl Eq. (4). A ligand redistribution or a additional methane abstraction must be involved because of the MeAl fragment in **4** [14].

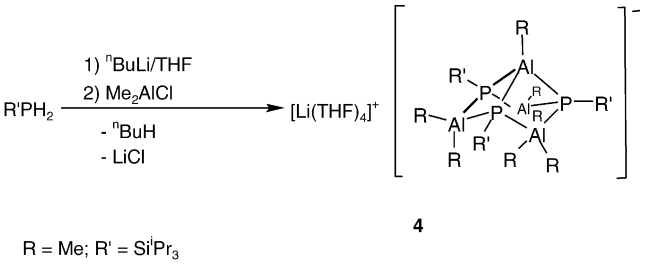

(4)

In **5**, $Li[AlH_4]$ is the starting material which was treated with the bulky arsane $R'AsH_2$ [$R' = Me_2(^iPrMe_2C)Si$] with evolution of H_2 Eq. (5) [15a].

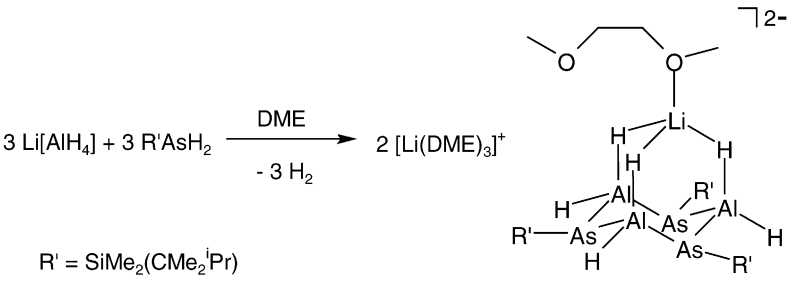

(5)

$Li_xM_yE_z$ cages with a rhombic dodecahedronal structure can be obtained in two ways. The heterocubane molecule $[MeAlNR'']_4$ ($R'' = 2,4,6\text{-}Me_3C_6H_2$) undergoes with LiP(H)R′ ($R' = {}^cHex$) a complete exchange of the group 15 ligand combined with a cage expansion involving Li^+ ions to give **6** [16] Eq. (6).

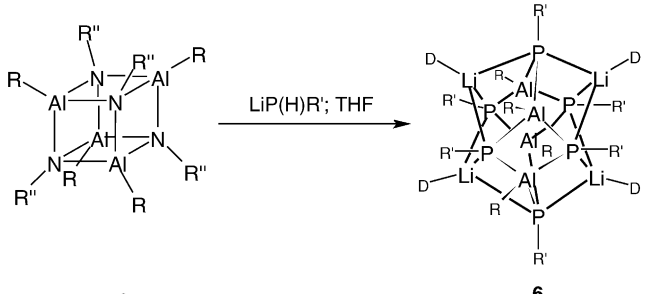

(6)

The second route is the reaction of $Li[AlH_4]$ with the bulky arsane $^iPr_3SiAsH_2$ which leads with evolution of H_2 to the $Li_4Al_4As_6$ cage compound **7** [12] Eq. (7). Compounds **6** and **7** contain donor solvent molecules to complete the coordination sphere of the Li^+ ions, THF for **6** and Et_2O for **7**.

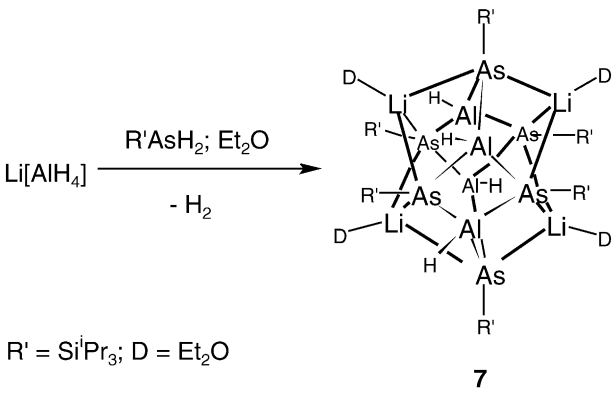

(7)

However, the shorter Al–P bonds in a corresponding $Li_4Al_4P_6$ cage enforces solvent-free Li^+ positions, synthesized from a six-membered Al–P compound by treatment with $^iPr_3SiPH_2$ and $AlMe_3$ Eq. (8) with evolution of methane to give **8** [14].

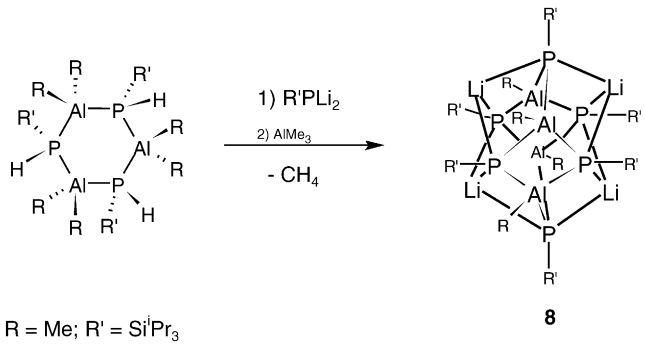

(8)

A totally different way to synthesize a Al–P cage compound was realized in the oxidative addition of a low valent Al compound like $(Cp^*Al)_4$ with elemental phosphorus to give $[P_4(Cp^*Al)_6]$ (**9**) according to Eq. (9) [17].

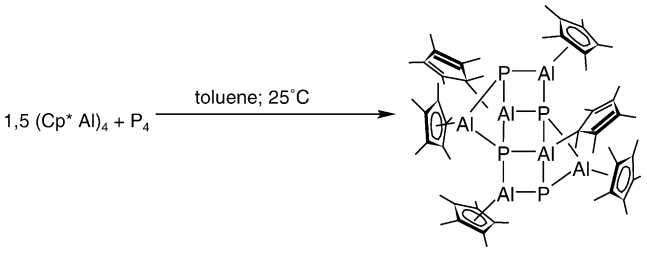

(9)

The reaction with $(Cp^*Al)_4$ with the tetraarsane $(^tBuAs)_4$ leads under As–C bond cleavage to $[(Cp^*Al)_3As_2]$ (**10**), a cluster with a formal *closo* structure Eq. (10) [18].

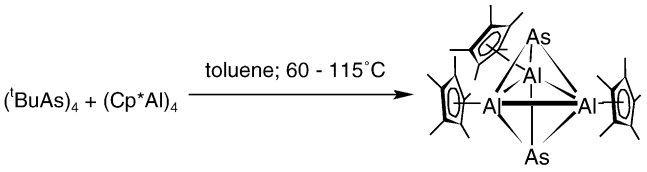

(10)

A complex with spirocyclic connection at two Al atoms and a K–Al–P net, **11**, is the result of the reaction of $AlCl_3$ with $K_2(^tBuPP^tBu)$ in Et_2O Eq. (11) [19].

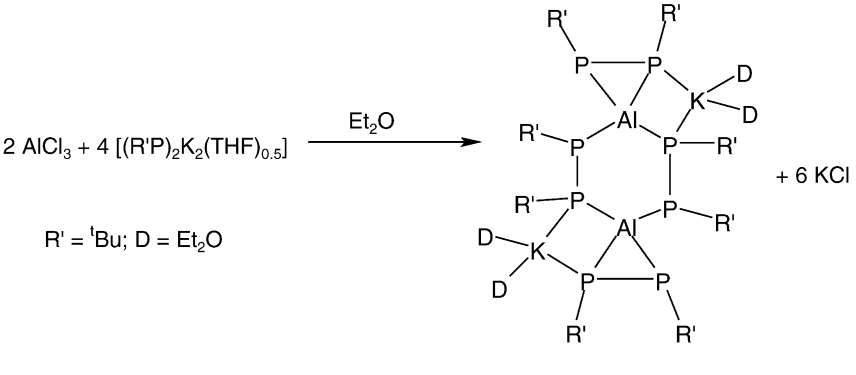

(11)

According to Table 1, ^{31}P NMR data depend mainly on the substituent at the P atom. All the examples shown possess silyl substituted phosphanido groups leading to high field signals −213 (**1**), −277 (**2a**) and −171 ppm (**2e**). The ^{27}Al NMR parameter of 46 ppm in **2a** is typical for coordination number (CN) four and hydride ligands. Similar results were observed for the arsanide heteroprismanes **2b** and **2c**. The heterocubane molecule **1** has a $\delta(^{27}Al)$ of 20 ppm. The chlorine ligands in **2e** cause a low field shift to 135 ppm.

The Al–H stretching vibrations νAlH for the terminal Al–H functions are useful probes in **2**. Values are given e.g. for **2a** with 1828 cm^{-1} and for **2b** with 1812 cm^{-1} [12].

Table 2 shows a comparison of M–E distances. Compound **1** is a typical heterocubane structure (Fig. 1) observed very often in inorganic and organometallic cage structures while

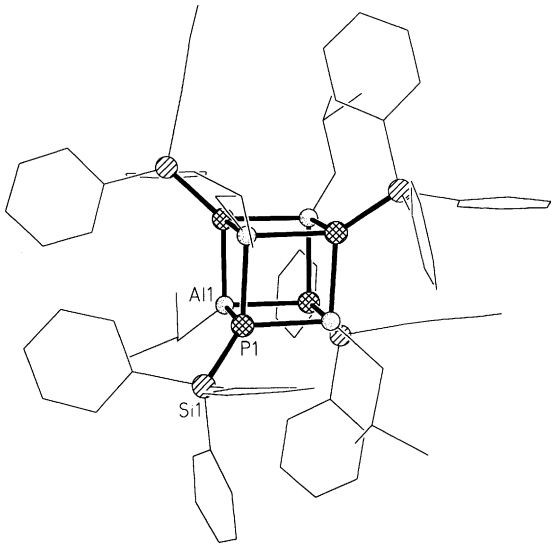

Fig. 1. Heterocubane structure of **1** (the organic ligands are drawn as thin lines for clarity) [11].

2a–e can be derived from the Wurtzite structure (Figs. 2 and 3). The Al–E bond lengths depend on the CN of the Al and E atoms, on the polarity of the Al–E bond, on the steric demand of the substituents and on electronical effects such as the electronegativity of the bound groups. The average value in **1** is 241 pm [11] and therefore in the region of the Al–P bond values of the Al_6P_6 heteroprismane compounds (see Table 2).

Compund **3** can be derived from a heteroprismane skeleton which is topped by one unit R′P and one unit HAl. In other words, it is a part of the Wurtzite structure capped with two heterocubane fragments (Fig. 4).

The anion in **4** formally contains a part of the structural motif of **3**; the six-membered ring is capped with an additional RAl unit (Fig. 5).

The structural motif of the dianion in **5** [15a] can be derived from the Zinc Blende structure or the adamantane if one counts the hydride functions as complex building units to give a $LiH_3Al_3As_3$ cage. Compound **5** is also a good example for the importance of the CN at compared atoms.

Table 1
^{31}P and ^{27}Al NMR shifts of M–E cage compounds

Compound	δ(^{31}P) (ppm)	δ(^{27}Al) (ppm)	Reference
$[^{i}BuAlPSiPh_3]_3$ (**1**)	−213.0	20.0	[11]
$[HAlPSi^{i}Pr_3]_6$ (**2a**)	−277.0	46.0	[12]
$[HAlAsSi^{i}Pr_3]_6$ (**2b**)		48.0	[12]
$[HAlAsSiMe_2(CMe_2{}^{i}Pr)]_6$ (**2c**)		40.0	[12]
$[MeAlPSi^{i}Pr_3]_6$ (**2d**)	−235.0	46.0	[14]
$[ClAlPSi^{i}Pr_3]_6$ (**2e**)	−171.0	135.0	[13]
$[Li(THF)_4][\{Me_2Al\}_3\{MeAl\}\{PSi^{i}Pr_3\}_3]$ (**4**)	−280.9	48.0	[14]
$[Li(DME)_3]_2[\{Li(DME)\}\{AlH_2\}_3\{AsSiMe_2(CMe_2{}^{i}Pr)\}_3]$ (**5**)		132.3	[15a]
$[\{Li(THF)\}_4\{AlMe\}_4\{P^{c}Hex\}_6]$ (**6**)	86.7		[16]
$[\{Li(OEt_2)\}_4\{AlH\}_4\{AsSi^{i}Pr_3\}_6]$ (**7**)		51.0	[12]
$[Li_4\{AlMe\}_4\{PSi^{i}Pr_3\}_6]$ (**8**)	−319	36	[14]
$[\{Li(OEt_2)_2\}\{(Ga^{t}Bu)(PBu^{t})_2(Ga^{t}Bu_2)\}]$ (**12**)	−77.0		[24]
$[(Ga^{t}Bu)(PBu^{t})_2(Ga^{t}Bu_2)_2]$ (**13**)	−80.0		[24]
$[^{t}BuGaPSiPh_3]_4$ (**14**)	−185.0		[11]
$[^{i}PrGaP^{t}Bu]_4$ (**15**)	−12.8		[25]
$[MesGaP^{t}Bu]_4$ (**16**)	1.5		[25]
$[\{MesGa\}_3\{GaP(H)^{t}Bu\}\{P^{t}Bu\}_4]$ (**17**)	−64.3, −9.0, 3.5[a]		[25]
$[\{MesGa\}_3\{GaP(H)Mes\}\{PMes\}_4]$ (**18**)	−147.4, −46.5, −45.2[b]		[26]
$[Cp(CO)_2FeGaPSiMe_3]_4$ (**19**)	−53.9		[28]
$[\{(Me_3Si)_3CGa\}_3P_4]$ (**20**)	−202.8, −521.9[d]		[30]
$[\{RGa\}_3(Ga)\{PAd\}_4\{P(H)Ad\}]$ (**21**)[c]	−80.3, −67.8, 31.4, 46.0		[31]
$[^{i}PrInPSiPh_3]_4$ (**25**)	−168.0		[36]
$[EtInPSi^{i}Pr_3]_4$ (**26**)	−189.0		[37]
$[MesInPMes]_4$ (**27**)	−75.5		[27]
$[\{(C_5H_5)(CO)_3Mo\}InPSiMe_3]$ (**29**)	−137.7		[39]
$[EtInPSiMe_2Thex]_6$ (**33**)	−166.9		[37]

[a] A_3MX spin system: $^{2}J(PP) = 213$ Hz, $^{1}J(PH) = 186$ Hz.
[b] A_3MX spin system: ^{2}J (PP) not observed, $^{1}J(PH) = 180$ Hz.
[c] R = $^{i}Pr_3C_6H_2$.
[d] AX_3 spin system: −202.8 d, −521.9 q, $^{2}J(PP) = 31$ Hz.

The Al–As bond length in $[Me_2AlAsPh_2]_3{\cdot}2$toluene [15b] is 252 pm; both of the atoms possess CN 4. In comparison $[RAlAsPh]_3{\cdot}Et_2O$ [15c] exhibits a Al–As distance of 243 pm caused by CN 3 for Al and As. Although the arsenic atoms in **5** have CN three an average Al–As bond length of 247 pm was observed probably due to the steric bulk of the silyl groups (Fig. 6). The CN 4 at the Al atoms may also be an additional factor.

Compound **6** possesses crystallographic C_i symmetry (Fig. 7) [16]. Every P atom in the rhombic dodecahedral $Li_4Al_4P_6$ cage is surrounded by an organic substituent and four metal atoms, two Li and two Al atoms in a

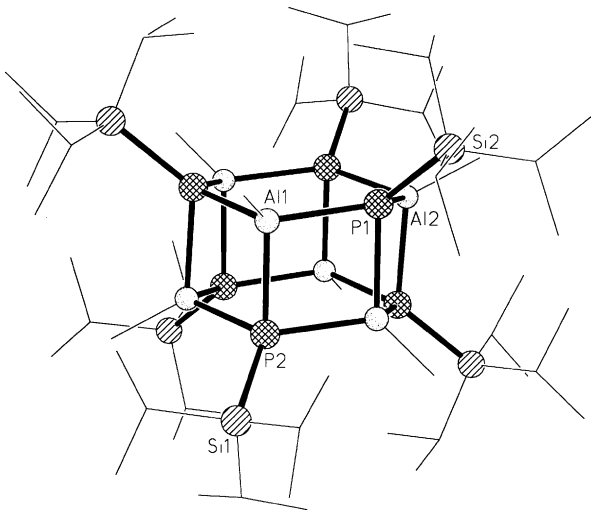

Fig. 2. Heteroprismane structure of **2d** [14].

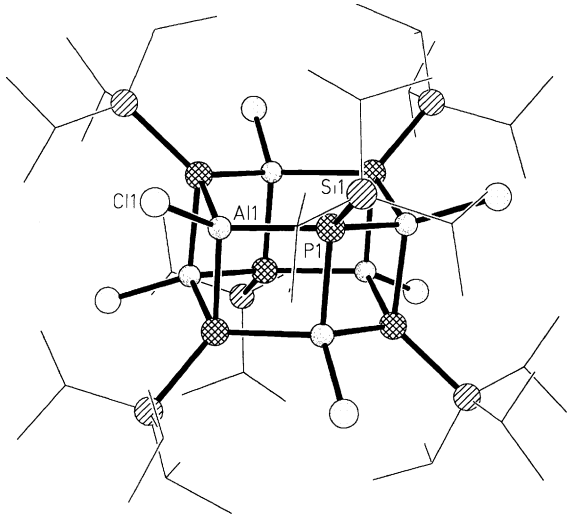

Fig. 3. Molecular structure of **2e** [13].

Table 2
Comparison of the M–E bond lengths in M–E cage compounds

Compound	M–E (pm)	Coordination number		Reference
		M	E	
$[^{i}BuAlPSiPh_3]_3$ (**1**)	241	4	4	[11]
$[HAlAsSi^{i}Pr_3]_6$ (**2b**)	248	4	4	[12]
$[MeAlPSi^{i}Pr_3]_6$ (**2d**)	237.9 (2)	4	4	[14]
$[ClAlPSi^{i}Pr_3]_6$ (**2e**)	241	4	4	[13]
$[HAlPSiMe_2(CMe_2{}^{i}Pr)]_7$ (**3**)	239.5 (6)	4	4	[14]
$[(Me_3N)HAlAsSi^{i}Pr_3]_2$	245	4	3	[12]
$[Li(THF)_4][\{Me_2Al\}_3\{MeAl\}\{PSi^{i}Pr_3\}_3]$ (**4**)	242.2 (3)	4	4	[14]
$[Li(DME)_3]_2[\{Li(DME)\}\{AlH_2\}_3\{AsSiMe_2(CMe_2{}^{i}Pr)\}_3]$ (**5**)	247	4	3	[15a]
$[\{Li(THF)\}_4\{AlMe\}_4\{P^{c}Hex\}_6]$ (**6**)	240	4	5	[16]
$[\{Li(OEt_2)\}_4\{AlH\}_4\{AsSi^{i}Pr_3\}_6]$ (**7**)	250	4	5	[12]
$[Li_4\{AlMe\}_4\{PSi^{i}Pr_3\}_6]$ (**8**)	242.5 (2)	4	4	[14]
$[P_4(Cp^*Al)_6]$ (**9**)	233	[a]	3	[17]
	241	[a]	4	
$[(Cp^*Al)_3As_2]$ (**10**)	248	4	3	[18]
$[\{Li(OEt_2)_2\}\{(Ga^{t}Bu)(PBu^{t})_2(Ga^{t}Bu_2)\}]$ (**12**)	245	4	4	[24]
	229	3	4	
$[(Ga^{t}Bu)(PBu^{t})_2(Ga^{t}Bu_2)_2]$ (**13**)	249	4	4	[24]
	234.4 (2)	3	4	
$[^{i}PrGaP^{t}Bu]_4$ (**15**)	242	4	4	[25]
$[\{MesGa\}_3\{GaP(H)^{t}Bu\}\{P^{t}Bu\}_4]$ (**17**)	244	4	4	[25]
	235	4	3	
$[\{MesGa\}_3\{GaP(H)Mes\}\{PMes\}_4]$ (**18**)	244	4	4	[26]
	232.7 (4)	4	3	
$[Cp(CO)_2FeGaPSiMe_3]_4$ (**19**)	243	4	4	[28]
$[\{(Me_3Si)_3CGa\}_3P_4]$ (**20**)	236	3	3	[30]
$[\{RGa\}_3(Ga)\{PAd\}_4\{P(H)Ad\}]$ (**21**)[b]	240	4	3/4	[31]
	231	3	3/4	
$[(GaR)_4(AsR')_6(GaR_2)(HAsPh)]$ (**23**)	250	3/4	3/4	[32]
$[Li(THF)_4]_2[(GaCl_2)_6(As^{t}Bu)_4]$ (**24**)	244	4	4	[33]
$[^{i}PrInPSiPh_3]_4$ (**25**)	259	4	4	[36]
$[EtInPSi^{i}Pr_3]_4$ (**26**)	257–258	4	4	[37]
$[MesInPMes]_4$ (**27**)	260	4	4	[27]
$[\{(C_5H_5)(CO)_3Mo\}InPSiMe_3]$ (**29**)	260	4	4	[39]
$[In_3(In_2)_3(PPh)_4(P_2Ph_2)_3Cl_7(PEt_3)_3]$ (**30**)	253–262	4	4	[38]
$[Li(THF)_4]_2[(InCl)_4(InCl_2)_2(As^{t}Bu)_6]$ (**31**)	263	4	3/4	[33]
$[EtInPSiMe_2Thex]_6$ (**32**)	257–263	4	4	[37]
$[(MesInCl)_4(InCl)_2(As^{t}Bu)_4]$ (**33**)	262	4/5	4	[40]
$[Li(THF)_4]_2[(PhCH_2InCl)_6(InCl)_2(As^{t}Bu)_6]$ (**34**)	263	4/5	4	[40]
$[Li(DME)_3]_2[(InMe_2)_2(InMe)_4(As^{t}Bu)_6]\cdot 2DME$ (**35**)	266	4	3/4	[40]
$[(InMe_2)_2(InMe)_6(As^{t}Bu)_6(OH)_2]\cdot 2THF$ (**36**)	263	4	4	[40]
$[(InMe)_9(As^{t}Bu)_8(OH)_2]\cdot 2.5THF$ (**37**)	265	4	4	[40]

[a] All CN 4; Al2 bound to two P atoms and one η^5-Cp* ligand.
[b] R = $^{i}Pr_3C_6H_2$.

square-pyramidal environment. Two of the P atoms have a *transoid* environment of the metal atoms and the other four a *cisoid* one. Nevertheless, there was only one broad ^{31}P NMR signal observed at 86.7 ppm indicating a fluctuating cage or very similar chemical shifts broadened by the quadrupole moment and the spin of ^{27}Al. Li and Al have CN 4. This leads to a mean Al–P value of 240 pm.

A difference in Al–As bond distances was noted between the *cisoid* dimer $[(Me_3N)HAlAsSi^{i}Pr_3]_2$ and the corresponding product **2b** (Fig. 8) because of the CN 3 of the As atoms in the dimer and CN 4 in the latter compound. In fact, 245 and 248 pm do not vary as much as might be expected perhaps because of the closer contact of the substituents in a four-membered ring.

Compound **7** has the same build-up principle as **6**. Li and Al atoms in the rhombic dodecahedral $Li_4Al_4As_6$ cage structure occupy the faces of an As octahedron. Interestingly, the more common arrangement of the building blocks in rhombic dodecahedra is a virtual octahedron of metal atoms upon where every triangular face is occupied by an electronegative heteroatom. Examples include $[(MesGa)_6F_4O_4]$ [20] and the core of the halides MX_2 (M = Mo, W; X = Cl–I) [10]. This structural correlation and inverse structure was also documented for M_xO_y and N_xLi_y skeletons [21]. In **7** the Al and As bridging mode leads to 250 pm for the Al–As bond lengths. The eight metal atoms in **6** and **7** form a pseudocube with three intercrossing C_2 axes and approximately D_{2h} symmetry for the rhombododecahedron (Fig. 9).

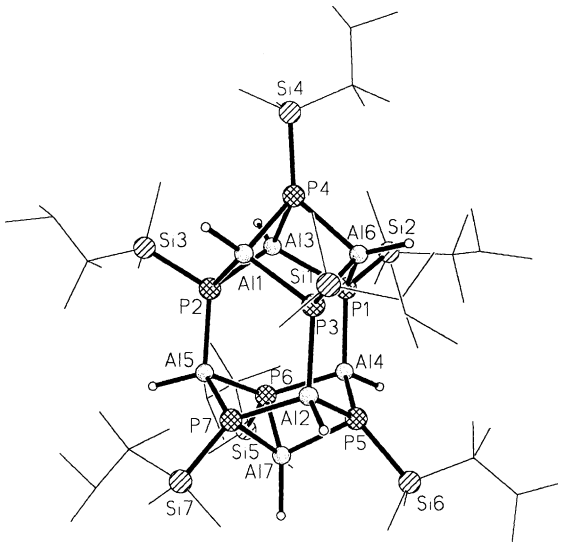

Fig. 4. Molecular structure of **3**. The central Al_6P_6 cage (Wurtzite type) is capped by a P and an Al atom, respectively [14].

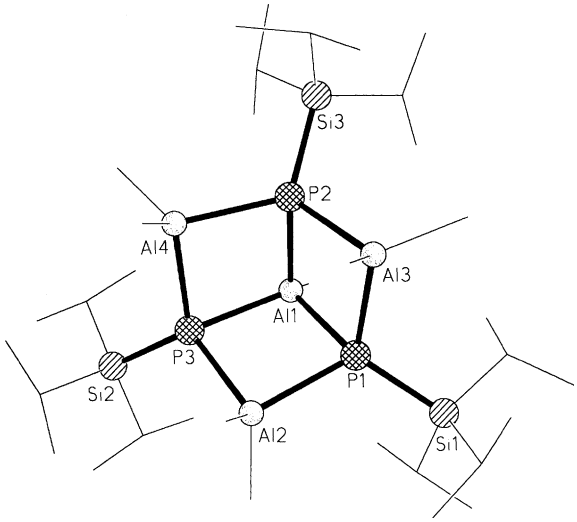

Fig. 5. Structure of the anion in **4** [14].

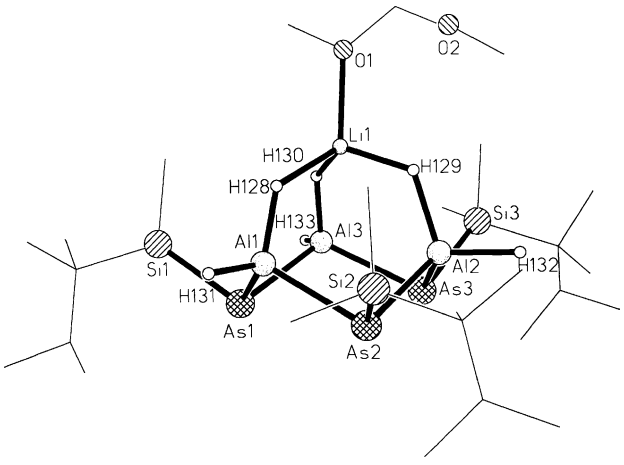

Fig. 6. Computer-generated plot of the dianion in **5** [15a].

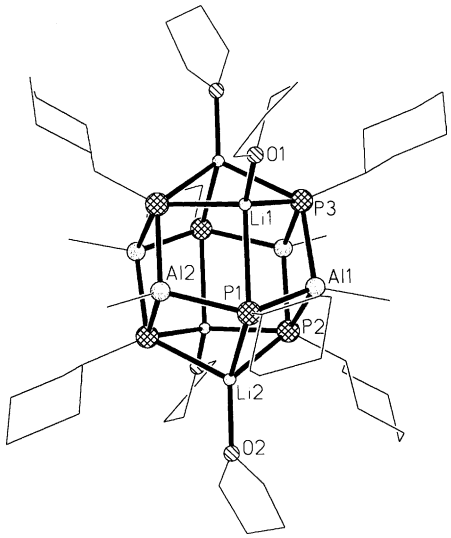

Fig. 7. Molecular structure of the rhombic dodecahedral molecule **6** [16].

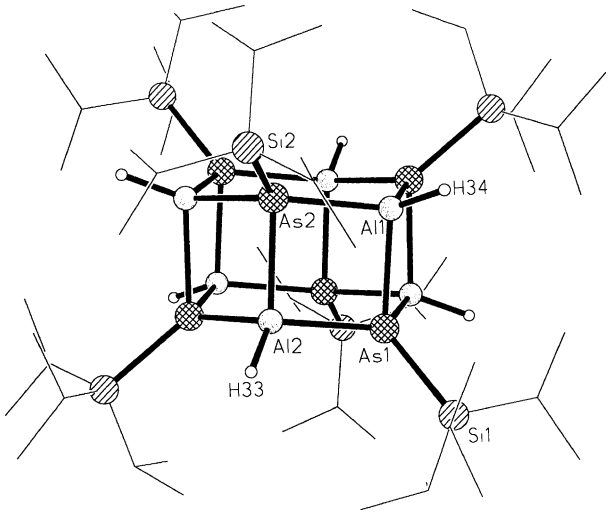

Fig. 8. Molecular structure of the heteroprismane **2b** [12].

The shorter Al–P (243 pm) and P–Li bonds in **8** in comparison to **6** is due to the protection of the Li^+ position by Si^iPr_3 groups leading to unoccupied coordination sites at Li^+ (Fig. 10) [14].

The result of Eq. (9) is an insoluble complex, consisting of two incomplete heterocubane fragments connected at one edge, $[P_4(Cp^*Al)_6]$ (**9**) [17]. The Cp^* ligands at Al act in a η^5 and a η^1 fashion, respectively (Fig. 11).

According to Fig. 12 the *closo* cluster $[(Cp^*Al)_3As_2]$ (**10**) possesses Al–As bond lengths of 248 pm and Al–Al bond lengths of 283 pm. The Al–As bond lengths are typical if one compares with electron precise Al–As cage compounds, while the Al–Al bonds are significantly longer than the bonds in $[(Me_3Si)_2CH]_2Al–Al[HC(SiMe_3)_2]_2$ (266 pm) [22] and in $(Cp^*Al)_4$ (277 ppm) [23].

Compound **11** is like **9** not soluble in organic solvents without decomposition. The K–Al–P can be described as spirocyclic complex consisting of a six-membered Al_2P_4

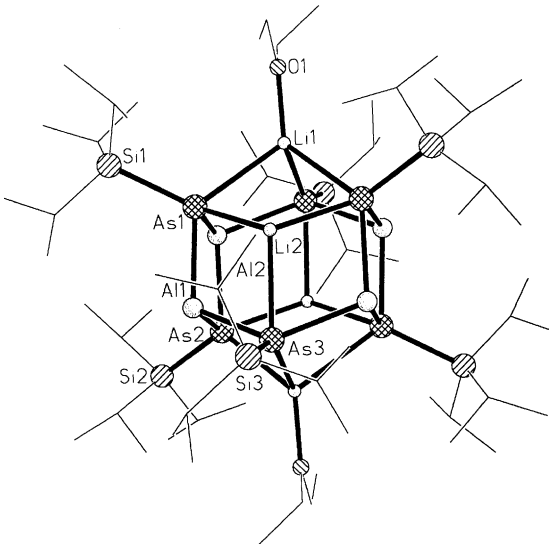

Fig. 9. Computer-generated plot of the rhombic dodecahedral molecule **7** (H positions of Al–H functions are not given in data base) [12].

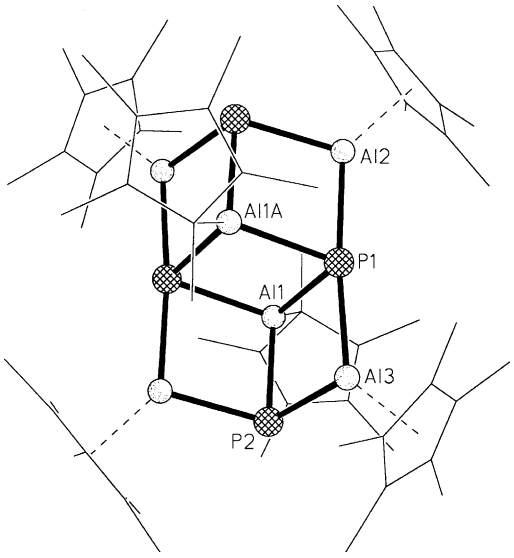

Fig. 11. Molecular structure of **9** [17].

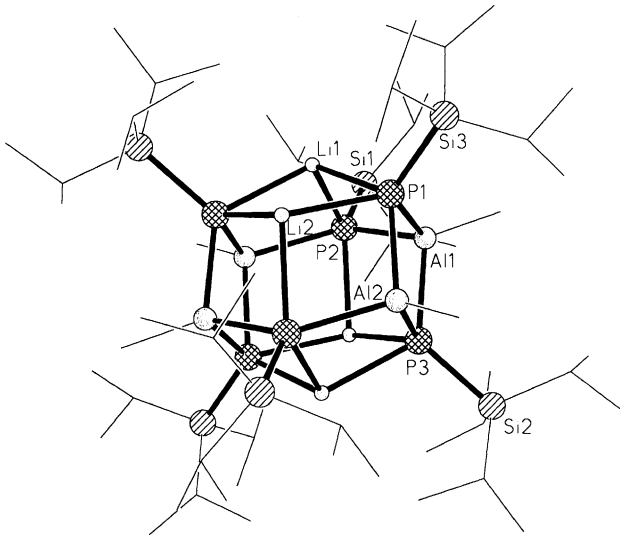

Fig. 10. Molecular structure of **8**. The Li^+ sites are not occupied by additional donor molecules [14].

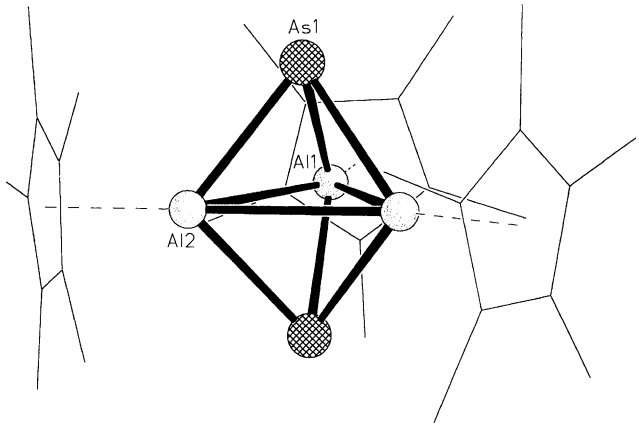

Fig. 12. *Closo* structure of the Al–As compound **10** [18].

ring connected with two P_2 units giving CN 4 for the Al atoms. One P atom of the three-membered AlP_2 ring and one of the six-membered ring is coordinated to the same potassium cation (Fig. 13) [19].

3. Gallium compounds

In principle, both synthetic routes used for the generation of Al–E cages can also be applied to build Ga–E frameworks. Sometimes the metathesis reaction to form M–E bonds is combined with a ligand redistribution, shown in Eq. (12) [24].

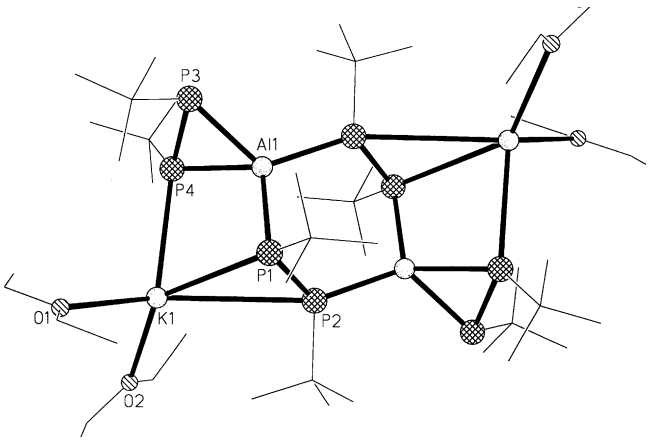

Fig. 13. Computer-generated plot of the K–P–Al spiro compound **11** [19].

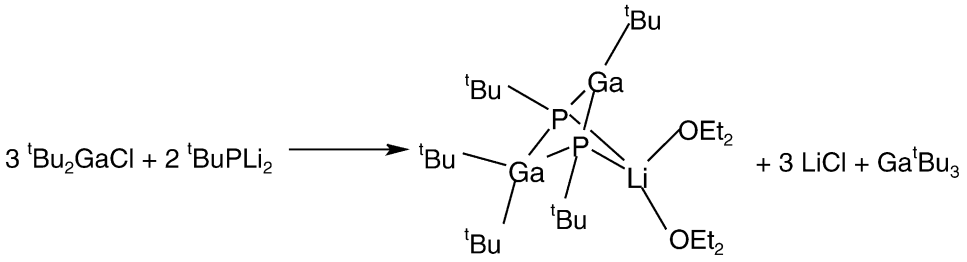

(12)

One equivalent of Ga^tBu_3 must be cleaved for the formation of **12** and **13**. These salt metathesis reactions are the key to a variety of Ga–E cages. However, a clean reaction was only observed when the substituents on Ga or E are bulky enough to prevent a polycondensation, which leads to creation of polymeric material [25–27]. Therefore, one does not observe aggregation of a intermediate RM = ER′ to form M–E cage compounds but, rather, in all cases the stepwise M–E bond formation with elimination of LiCl [24–27]. Heterocubane molecules are the typical result of such metathesis reactions Eq. (13).

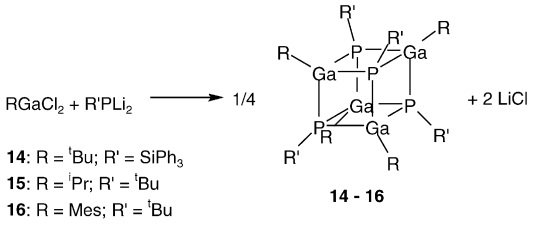

(13)

Complex **16** was only a by-product formed during the treatment of R′PLi_2 with a mixture of $RGaCl_2$ and $GaCl_3$ which yielded the asymmetrical heterocubanes [{RGa}$_3${GaP(H)R′}{PR′}$_4$] [R = Mes, R′ = ^{t}Bu (**17**) [25]; R = R′ = Mes (**18**) [26]; Eq. (14)]. The protons for the P(H)R′ units were delivered by the solvent (see also **21**).

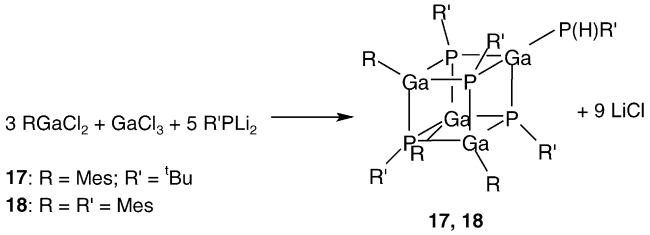

(14)

$[Cp(CO)_2Fe]_2GaCl$ and $KP(SiMe_3)_2$ are the starting materials for the formation of $[Cp(CO)_2FeGaPSiMe_3]_4$ (**19**). The salt $K[\{Cp(CO)_2Fe\}_2Ga–PSiMe_3]$ is a proposed intermediate after $P(SiMe_3)_3$ elimination which undergoes a salt elimination of $K[CpFe(CO)_2]$ to give **19** [28].

An oxidative addition reaction between $[(Me_3Si)_3CGa]_4$ [29] and P_4 gives the cage compound [{$(Me_3Si)_3CGa$}$_3P_4$] (**20**) according to Eq. (15) [30].

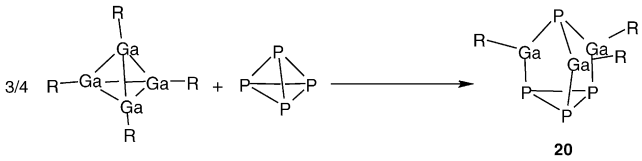

(15)

Ga–As double bonds indicated by short exocyclic Ga–As bonds of 231.8 (1) pm were found in the ring compound [{$Li(THF)_3$}$_2Ga_2${$As(Si^iPr_3)_3$}$_4$] which was synthesized from $GaCl_3$ and $Li_2AsSi^iPr_3$ [9].

An abstraction of protons together with ligand redistribution was observed during the combination of two very bulky reagents, $[RGaCl_2(THF)]$ and R′PLi_2 (R = $^iPr_3C_6H_2$; R′ = 1-adamantane (Ad)) [31] giving the tetranuclear complex [{RGa}$_3$(Ga){PAd}$_4${P(H)Ad}] (**21**). The heteroprismane $[HGaAsSi^iPr_3]_6$ (**22**) was prepared according (2) [12] proving the feasibility of H_2 evolution with gallium hydrid species. The first large structurally characterized Ga–As complex, $[(GaR)_4(AsR')_6(GaR_2)(HAsPh)]$ (**23**), was synthesized by a similar route, the elimination of $SiMe_4$, accomplished with the reagents $Ga(CH_2SiMe_3)_3$ and $PhAsH_2$ in Eq. (16) [32]. In addition, As–As bonds were formed, possibly with evolution of H_2.

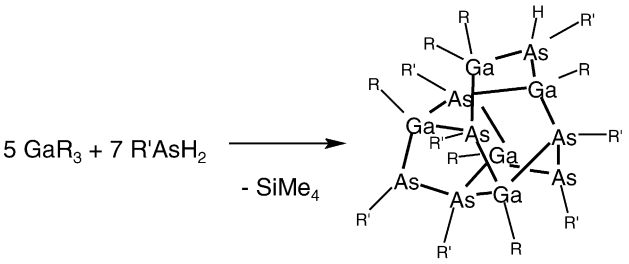

(16)

In contrast to (13) the reaction between $GaCl_3$ and $^tBuAsLi_2$ in the molar ratio 6:4 directly gives the salt $[Li(THF)_4]_2[(GaCl_2)_6(As^tBu)_4]$ (**24**) without generation of polymeric material Eq. (17). The dianion $[(GaCl_2)_6(As^tBu)_4]^{2-}$ has a heteroadamantane framework [33].

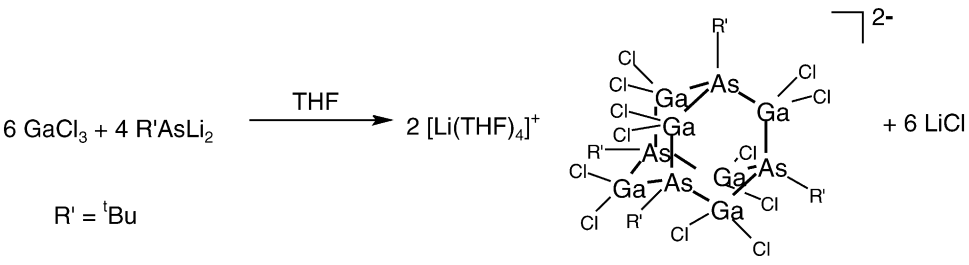

(17)

Only a singlet signal was expected for **14**–**16** and **19** in their ^{31}P NMR spectra (see Table 1). However, **17**, **18** and **21** should show a set of resonances, depending on the symmetry of the compounds in solution. Compound **17** exhibits a A_3MX spin system caused by the three different P atoms in the Ga_4P_5 framework. Three peaks in the ratio 3:1:1 (3.5, −9.0, −64.3 ppm) were observed for **17** and similar for **18** (−45.5, −46.5, −147.4 ppm), but only for **17** the corresponding coupling pattern was found [$^2J(PP) = 213$ Hz]. This is quite rare because of the quadrupole moment and the nuclear spin of Ga. Therefore, the coupling was assumed to be a "through space" interaction. Other examples of such coupling were found in a few Ga–P four- membered ring compounds [34,35] and in **20** [30]. Compounds **18** as well as **21** (−80.3, −67.8, 31.4, 46.0 ppm) exihibit no coupling pattern [26,31]. A comparison between the $\delta(^{31}P)$ values of the different P atoms indicates a rough correlation between the position of the signal and the bridging modus of the P atom: as more Lewis acidic metal atoms are bound to the pnicogen atom the resonance signal moves to lower field (always for one sort of substituent at the P atom). The P_4S_3-like cage compound **20** gives a AX_3 spin system in the ^{31}P NMR spectrum [30] in solution with a $^2J(PP)$ coupling constant of 31 Hz (see Table 2).

The variation of the Ga–P bond lengths in **15** are small because of the similarity of the ^{i}Pr and ^{t}Bu substituents leading to a rather undistorted Ga_4P_4 skeleton with an average Ga–P distance of 242 pm (Figs. 14 and 15) [25,28].

The additional external P(H)R′ group in **17** and **18** induces a distortion of the heterocubane structure but the mean value of 244 pm is comparable to the value in **15** (Figs. 16 and 17).

The lower CN of the terminal phosphanido ligand causes short Ga–P bonds of 235 (**17**) and 232.7 (4) pm (**18**) [25,26]. The differentiation by the CN is the main reason for rather variable Ga–E bond lengths. In **12** and **13** two categories of distances were observed (Figs. 18 and 19). CN 4 at Ga leads to 245 (**12**) and 249 pm (**13**) (Ga–P) while CN 3 shortens the value to 229 and 234.4 (2) pm [24].

A comparable situation was found in **21** with 231 and 240 pm (Fig. 20). For **23** the authors only gave an average Ga–As distance of 250 pm [32] (Fig. 21). The shortening for Ga–As in the heteroadamantane dianion of **24** to 244 pm (CN 4 for Ga and As) is due to the cumulation of electronegative ligands on the Ga atoms [33] (Fig. 22).

Compound **20** possesses a structure which can be structurally derived from P_4S_3 or the Zintl anion P_7^{3-} [30] with a rather short Ga–P distances of 236 pm caused by CN 3 on the Ga and the P atoms (Fig. 23).

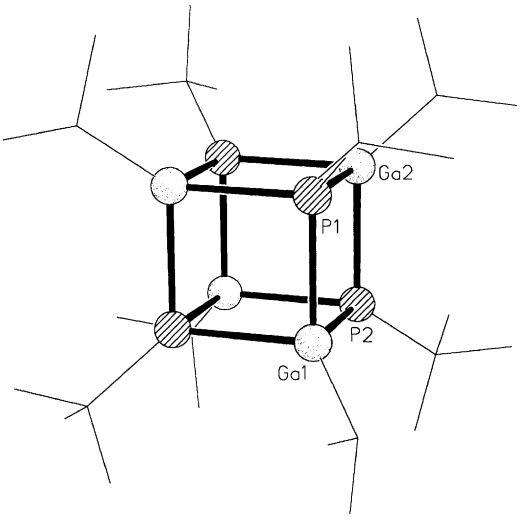

Fig. 14. Molecular structure of the heterocubane compound **15** [25].

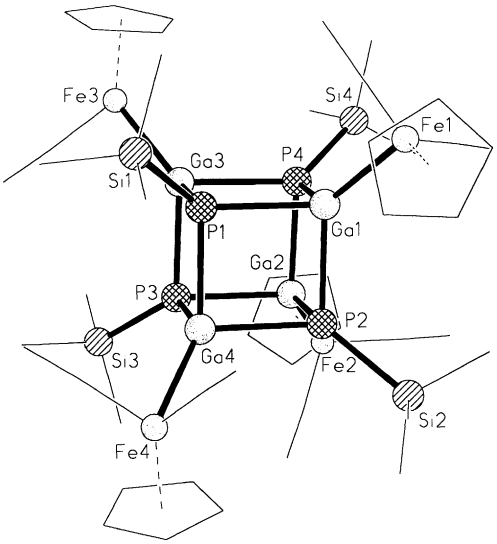

Fig. 15. Molecular structure of **19** [28].

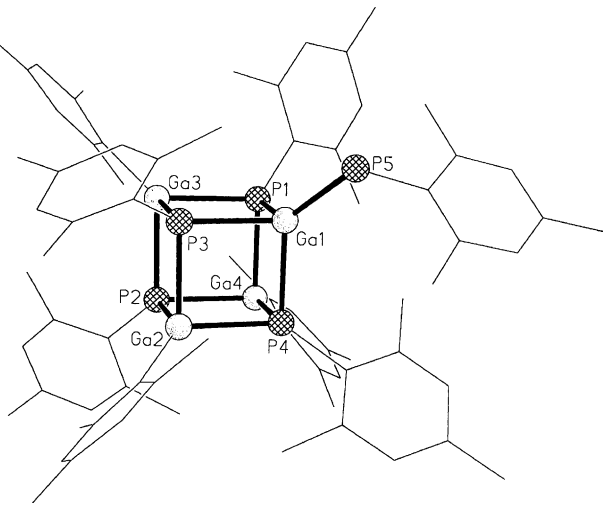

Fig. 17. Molecular structure of **18** [26].

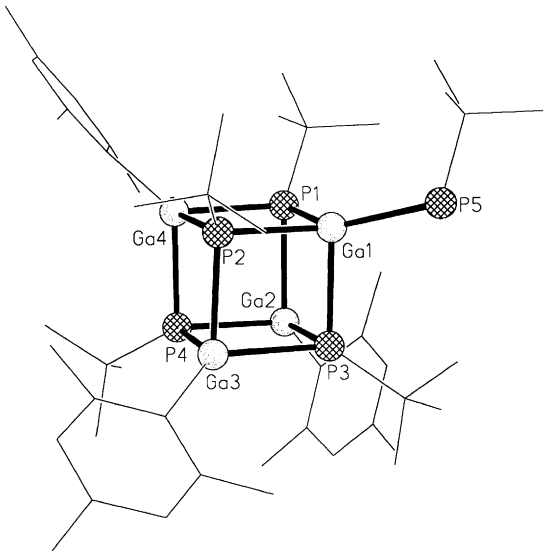

Fig. 16. Computer-generated plot of **17** with a slightly distorted heterocubane structure [25].

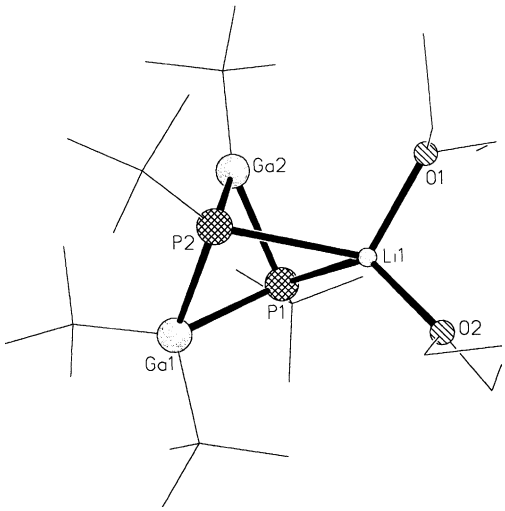

Fig. 18. Structure of the salt **12** [24].

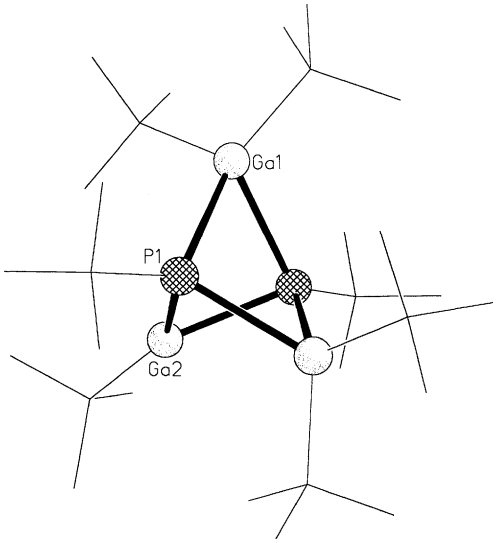

Fig. 19. Structure of the neutral compound **13** [24].

4. Indium compounds

Three synthetic routes can be adopted for the formation of heterocubane molecules with indium. The elimination of an alkane was used for the generation of $[^{i}PrInPSiPh_3]_4$ (**25**) [36] and $[EtInPSi^{i}Pr_3]_4$ (**26**) [37] Eq. (18) while $[MesInPMes]_4$ (**27**) was formed in a salt metathesis according to Eq. (13) [27]. Eq. (18) is also useful to obtain and isolate a corresponding In–As heterocubane, the $[EtInAsSi^{i}Pr_3]_4$ (**28**) [37].

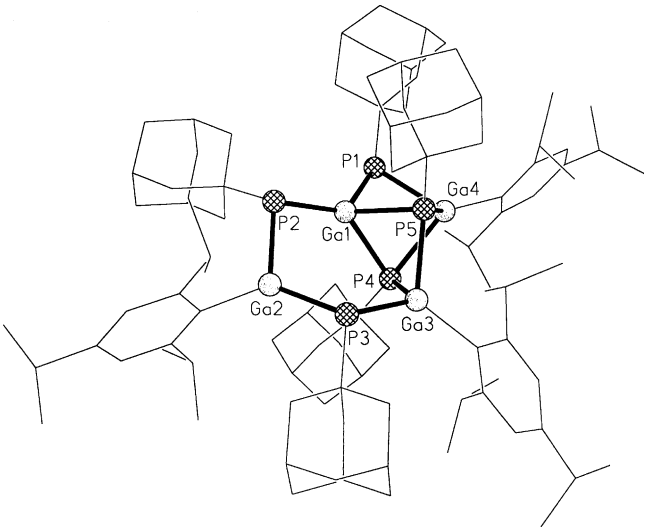

Fig. 20. Structure of the spirocyclic complex **21** [31].

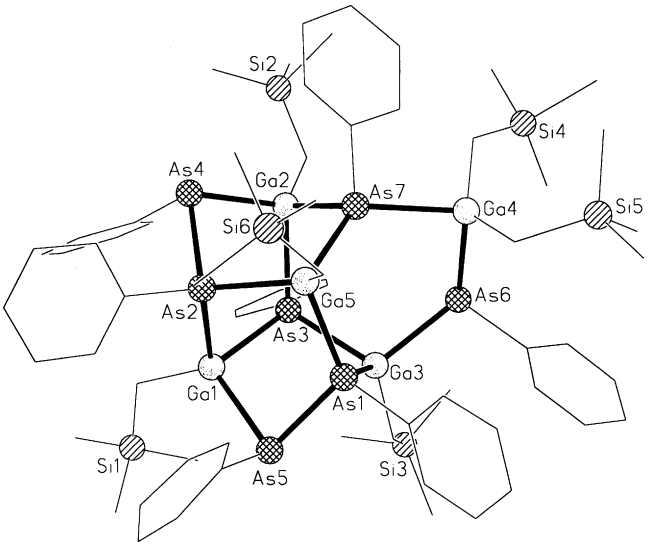

Fig. 21. Molecular structure of **23** [32].

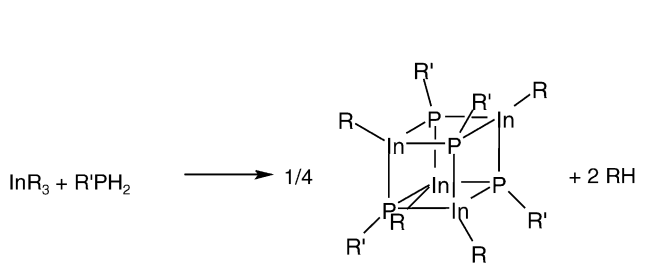

(18)

The third method, the elimination of Me_3SiCl, was applied to build-up the metalla-substituted complex $[\{(C_5H_5)(CO)_3Mo\}InPSiMe_3]$ (**29**) [39] Eq. (19).

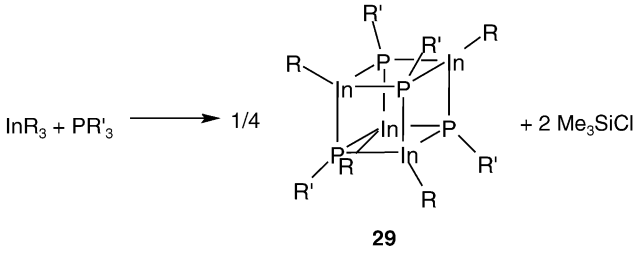

(19)

Compound $[In_3(In_2)_3(PPh)_4(P_2Ph_2)_3Cl_7(PEt_3)_3]$ (**30**) was obtained by the treatment of $InCl_3$ with $PhP(SiMe_3)_2$ in the presence of PEt_3 according to Eq. (20) [38].

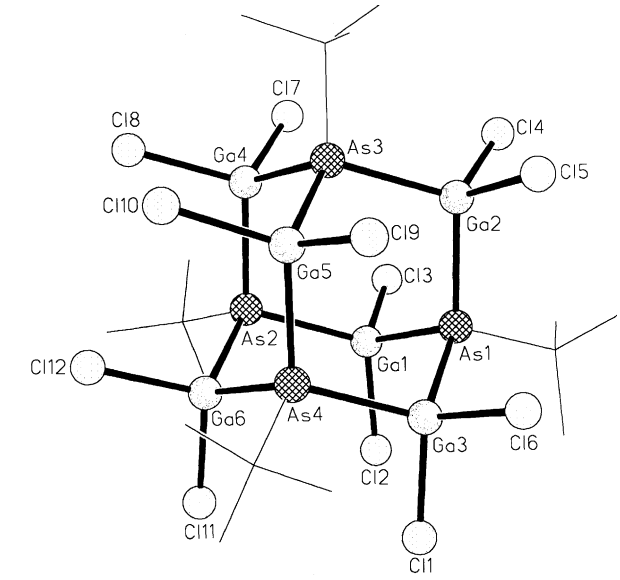

Fig. 22. Structure of the dianion in **24** derived from the Zinc Blende [33].

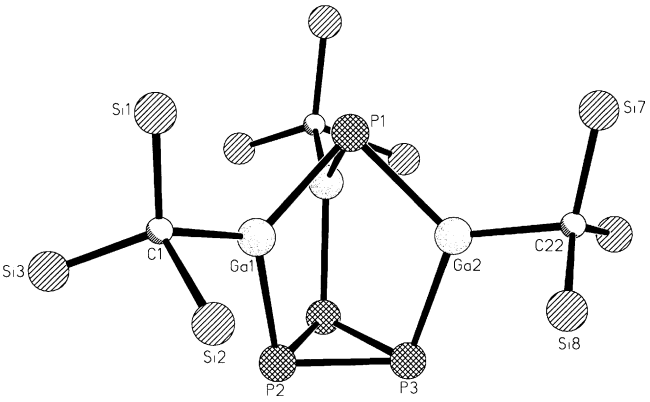

Fig. 23. The Ga_3P_4 cage in compound **20** is isostructural to P_4S_3 [30].

$$9\ InCl_3 + 3\ PEt_3 + 10\ PhP(SiMe_3)_2 \longrightarrow [In_3(In_2)_3(PhP)_4(Ph_2P_2)_3Cl_7(PEt_3)_3] + 20\ Me_3SiCl$$

30 (20)

Besides the loss of Me_3SiCl and the formation of In–P bonds, redox processes occur during the reaction which lead to the formation of additional P–P and In–In bonds [39].

An In_6As_6 cage was found when $InCl_3$ was treated with $^tBuAsLi_2$ in a molar ratio of 1:1 according to Eq. (21) [33]. The dianion in $[Li(THF)_4]_2[(InCl)_4(InCl_2)_2(As^tBu)_6]$ (**31**) can be derived from a heteroprismane by formal addition of two Cl^- ions.

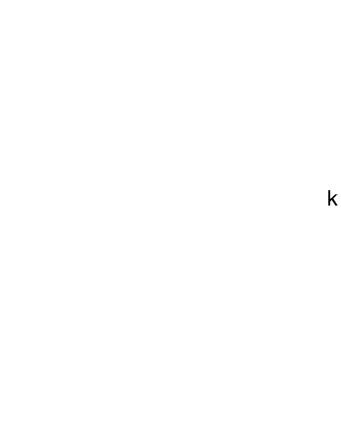

31

This In_6As_6 heteroprismane is still intact in $[RInPR']_6$ (**32**; R = Et; R = $SiMe_2Thex$) [37] generated from $InEt_3$ and H_2PR' by the elimination of an alkane Eq. (22).

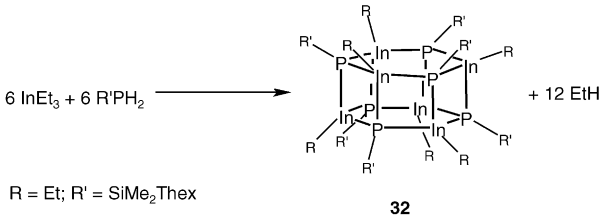

32 (22)

In order to expand the size of the In–E cages, mixtures of organochlorometallanes and $InCl_3$ were treated with Li_2As^tBu. The reaction of $MesInCl_2$ and $InCl_3$ with Li_2As^tBu in a molar ratio of 4:2:4 gives the neutral complex $[(MesInCl)_4(InCl)_2(As^tBu)_4]$ (**33**) according to Eq. (23) [40].

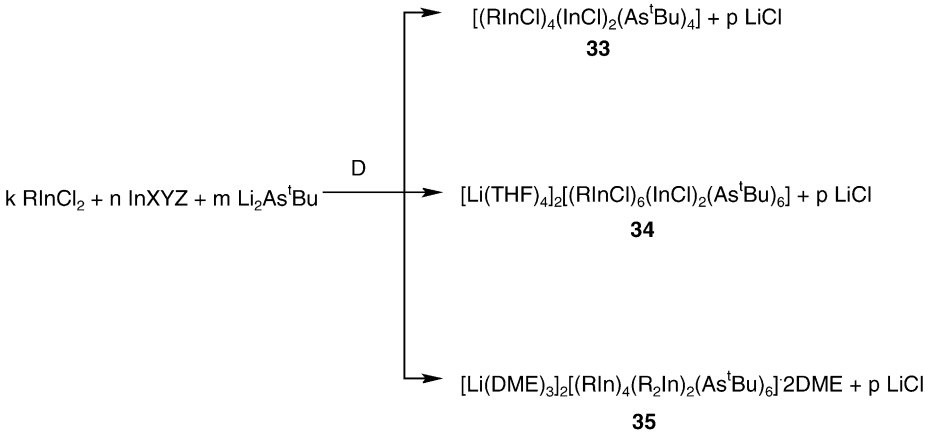

33: R = Mes; X = Y = Z = Cl; k = 4; n = 2; m = 4; D = Et_2O; p = 8
34: R = $PhCH_2$; X = Y = Z = Cl; k = 6; n = 2; m = 6; D = THF; p = 10
35: R = Me; X = Y = Me; Z = Cl; k = 4; n = 2; m = 6; D = DME; p = 10 (23)

The combination of $PhCH_2InCl_2$, $InCl_3$ and Li_2As^tBu in a ratio of 6:2:6 on the other hand leads to a salt with a dianion, $[Li(THF)_4]_2[(PhCH_2InCl)_6(InCl)_2(As^tBu)_6]$ (**34**) Eq. (23) [40]. An asterane-like dianion is the result of the combination of Me_2InCl, $MeInCl_2$ and Li_2As^tBu (2:4:6) in DME giv-

ing $[Li(DME)_3]_2[(InMe_2)_2(InMe)_4(As^tBu)_6]\cdot 2DME$ (**35**) Eq. (23).

In a recent paper, it was shown that the partial hydrolysis of group 13 compounds leads to cage-expansion reactions [41]. This method was also applied in 13/15 chemistry [40]. After reaction of Me_2InCl, $MeInCl_2$ and Li_2As^tBu in a ratio of 2:6:6 only a microcrystalline powder could be isolated. After addition of small amounts of wet THF the octanuclear complex $[(InMe_2)_2(InMe)_6(As^tBu)_6(OH)_2]\cdot 2THF$ (**36**) was formed. This method was also successful in the reaction of $MeInCl_2$ and Li_2As^tBu with the ratio of 1:1. A nonanuclear cage molecule $[(MeIn)_9(As^tBu)_8(OH)_2]\cdot 2.5THF$ (**37**) was obtained in good yield [40] Eq. (24).

Compounds **25–29** possess weakly distorted In_4P_4 heterocubane skeletons with quite similar In–P distances of 259–260 pm (see Table 2; Figs. 24–27).

The In-P cage in **30** consists of six- and five-membered rings containing In–P, In-In and P–P bonds. For every In–In bond (mean value 274 pm) a P–P bond (mean value 222 pm) was formed. According to a count of the valence electrons (54 VE) all 27 bonds of the cage are 2-center-2-electron bonds leading to an electron precise description of the complex skeleton. The cage is centered by a Cl^- ion. However, theoretical calculations have shown that the central Cl^- ion is not necessary for the stability of the cage [38]. The shortest

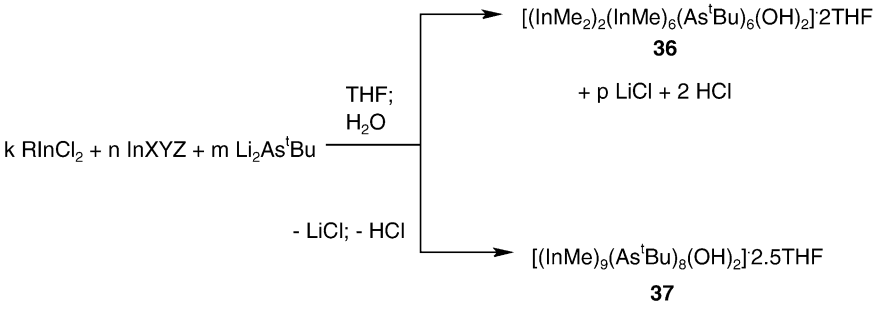

36: R = Me; X = Y =Me; Z =Cl; k = 6; n = 2; m = 6; p = 12
37: R = Me; k = 1; n = 0; m = 1

(24)

Only a singlet was expected for the heterocubane molecules **25–29** (see Table 1) because of their symmetry. The ^{31}P NMR signal of **25** receives another downfield shift to −168.0 ppm in comparison to the resonances of **1** (M = Al) and **14** (M = Ga). However, there is no simple rule to unterstand the trend in the $\delta(^{31}P)$ values because of the interaction of many parameters to the P atoms like bond angles, electronic influence of the bound metal atom and the substituents on the metal atom.

distances to the next indium atoms are 307, 303 and 301 pm (Fig. 28).

Surprisingly, the In–As distances in **31** are only 3 pm longer than in **25–29**, although one should expect a lengthening of approximately 10 pm when compared with the In–P bonds. The reason again must be mainly the electronegative chlorine ligands on the indium [33]. The structure of the dianion in **31** (Fig. 29) is related to the Wurtzite struc-

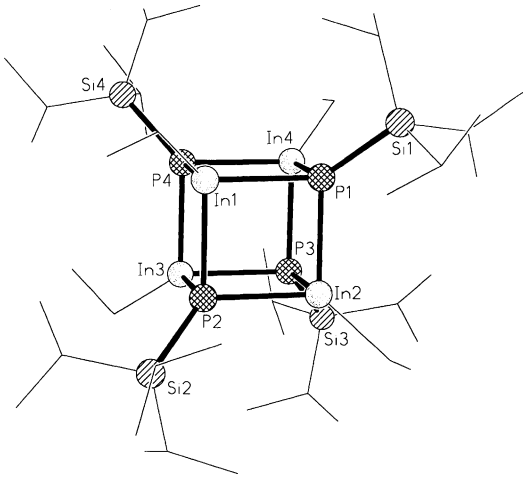

Fig. 24. Molecular structure of the heterocubane compound **26** [36].

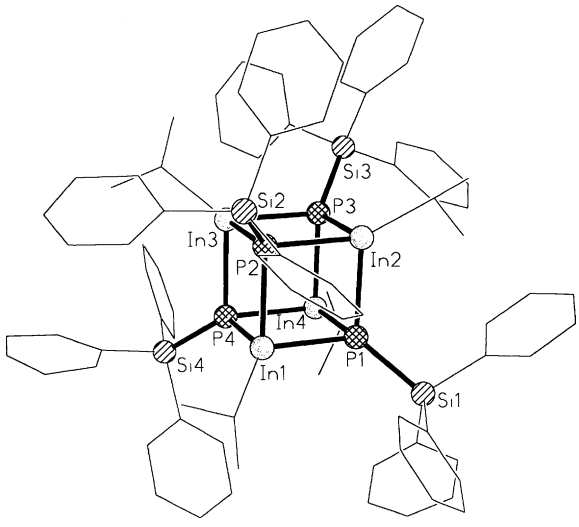

Fig. 25. Molecular structure of **25** [37].

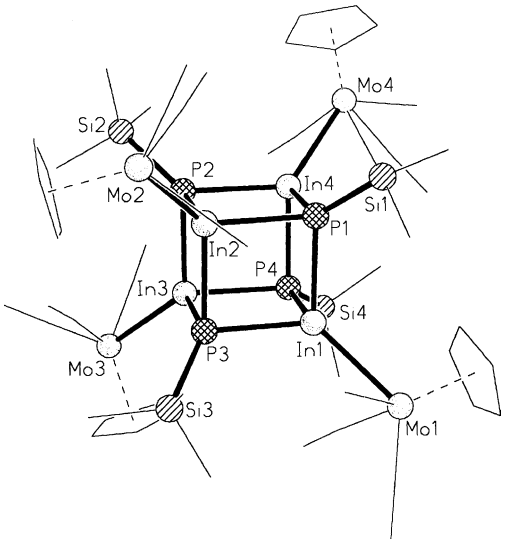

Fig. 26. Heterocubane compound **29** with In–Mo bonds [39].

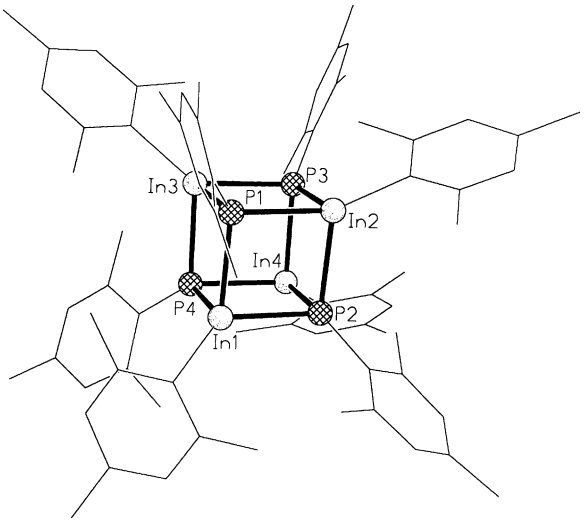

Fig. 27. Plot of the homoleptic substituted heterocubane compound **27** [27].

ture and to asterane-type molecules like the carbosilane $[Cl_2Si(CH)_2(SiCl)_2CH_2]_2$ [42].

The intact heteroprismane **32** possesses slightly longer In-P bonds (highest value 258 pm) than the values observed in the heterocubane molecule **26** (highest value 263 pm) because of the bulky $SiMe_2Thex$ ligands (Thex = $–CMe_2CMe_2$) (Fig. 30).

The C_2-symmetrical In–As–Cl skeleton of **33** can be derived from a rhombic dodecahedron if one creates four additional In–Cl bonds (e.g. In2···Cl2a). The six indium atoms form an octahedron and all eight faces of the octahedron are occupied by Cl and As atoms (Fig. 31) [40].

The dianion in **34** does not fit in a simple scheme. The structural motif is a D_{3d}-symmetrical In–As–Cl cage built-up by a hexagonal–bipyramidal In core. The atoms of the basal plane are bridged alternatively by Cl and As

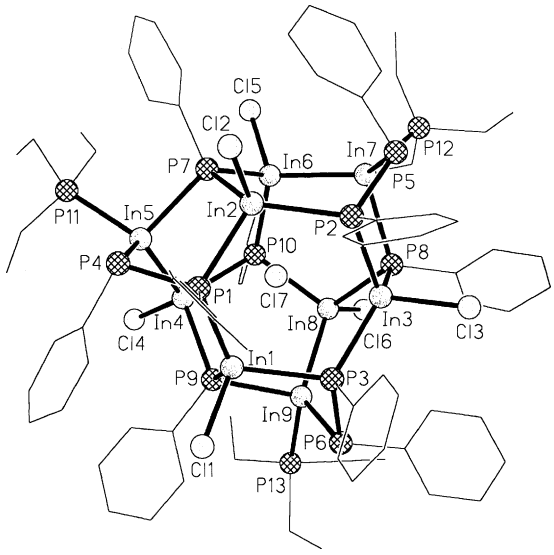

Fig. 28. Molecular structure of **30** with an included Cl^- ion [38].

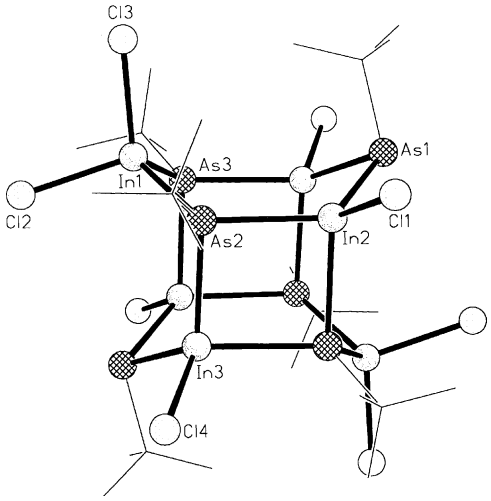

Fig. 29. Structure of the dianion in **31** [33].

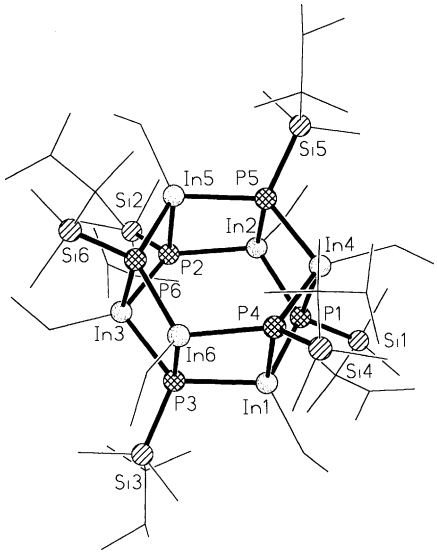

Fig. 30. Plot of the heteroprismane compound **32** [37].

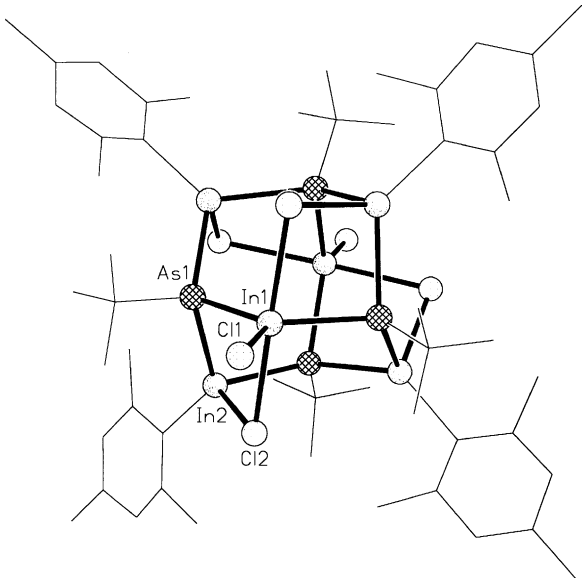

Fig. 31. Structure of the neutral In–As–Cl cage compound **33** [40].

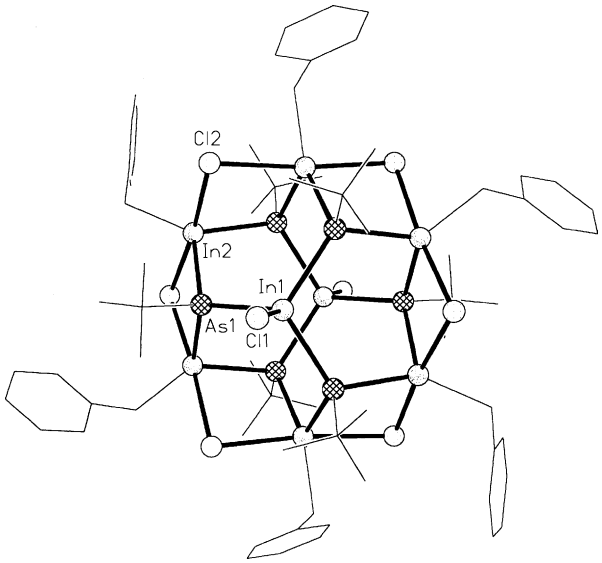

Fig. 32. Structure of the dianion in **34** [40].

atoms above and below every In–In edge. The As atoms are coordinated to the apical indium atoms. Together a network of four- and six-membered rings is formed (Fig. 32) [40].

In contrast, the dianion in **35** can be derived directly from a heteroprismane at which two edges were opened by Cl^- ions. The C_{2h}-symmetrical In–As cage is comparable to the In–As cage in **21** (Fig. 33). The long In–As bonds (267 and 269 pm) on In2 are remarkable. This can be explained by the two negative charges on the In–As cage and the two bulky ^{t}Bu groups on As2 and As2a causing the elongation of the In–As bonds.

In **36** the asterane motif of **31** and **35** is bridged and closed by two units Me_2InOH. At every OH function a THF molecule is bound via hydrogen bridging (Fig. 34). This

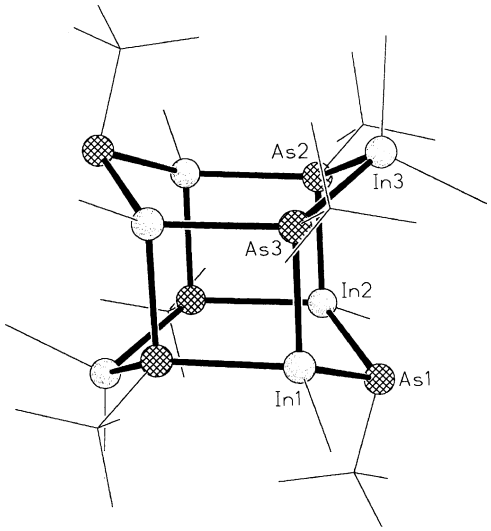

Fig. 33. Structure of the dianion in **35** with asterane structure [40].

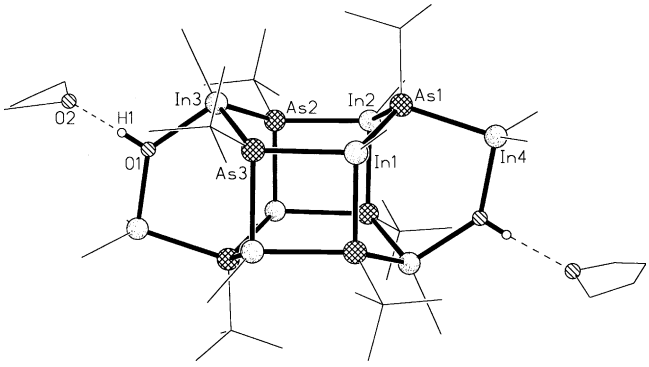

Fig. 34. Molecular structure of **36** containing two Me_2InOH units [40].

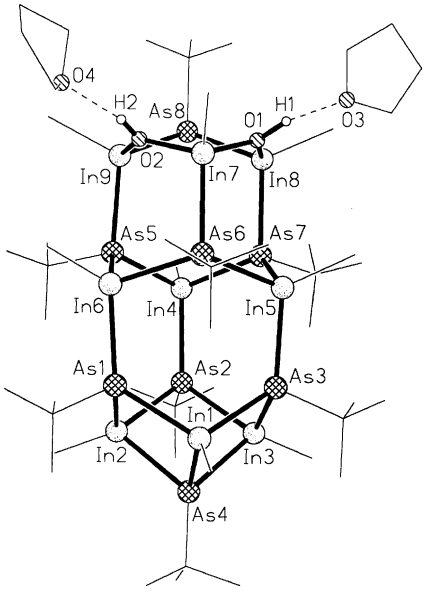

Fig. 35. Structure of the nonanuclear neutral complex compound **37** [40].

reduces the In–As distances at In3 to an average value of 261 pm.

The basis of the In–As–O cage in **37** is a part of the Wurtzite structure. The open side of the six-membered tube is capped with an As^{t}Bu unit leading to a heterocubane fragment (Fig. 35). The other side of the tube is not capped but two THF molecules are bound to the OH groups. Interestingly, the OH funtions act as substitute for the As^{t}Bu groups. However, the influence of the O atoms leads to narrowing of the six-membered ring and to short In–As bonds (e.g. In9–As8 259 pm).

5. Conclusion

In general, the derivation of the M–E cages from basic structural motifs like heterocubanes, heteroprismanes or heteroadamantanes seems to be typical for electron-precise compounds in 13/15 chemistry. The heteroprismane and the heteroadamantane motif point directly to the Wurtzite and the Zinc Blende structure, respectively. When a third element such as lithium is involved in the cage build-up, a rhombic dodecahedron is the preferred polyhedron (see e.g. **7** and **8)**. Only the dianion of **34** does not fit this simple scheme.

When the oxidation state of M and E differs from three a large variety of M–E cages can be observed. Examples are the compounds **9**, **11**, **20**, **23** and **30**. For electronically non-precise compounds Wade's rules are helpful, shown for the *closo* cluster of **10**.

In the compounds discussed the M–E bond lengths vary mostly with the CN of the participating elements. Other reasons are the oxidation state of the elements or the electronegativity of atoms or substituents as well as the bulk of substituents, but coordination number is the most important. Clear examples are **9** (Al–P: 233 pm versus 241 pm), **12** (Ga–P: 229 pm versus 245 pm), **13** (Ga–P: 234 pm versus 249 pm) or **21** (Ga–P: 231 pm versus 240 pm) with a strong dependence of the M–P bond on CN (see Table 2). As expected, the difference between Al–P(As) and Ga–P(As) is not very significant because of the d-electron contraction, while the In-P(As) bonds are about 15–20 pm longer in comparison to the previous examples.

Acknowledgements

The authors are grateful to the Deutsche Forschungsgemeinschaft for financial support.

References

[1] A.J. Downs (ed.), Chemistry of Aluminium, Gallium and Indium, Blackie Academic and Professionals, London, 1993.
[2] M. Driess, Adv. Inorg. Chem. 50 (2000) 235.
[3] A.H. Cowley, Angew. Chem. Int. Ed. Engl. 28 (1989) 1208.
[4] A.H. Cowley, J. Organomet. Chem. 400 (1990) 71.
[5] P.P. Power, Chem. Rev. 99 (1999) 3463.
[6] P.J. Brothers, P.P. Power, Adv. Organomet. Chem. 39 (1996) 1.
[7] (a) For organometallic compounds see: Gmelin Handbook of Inorganic Chemistry, Gallium, Organogallium Compounds. Part 1. Springer, Berlin, New York, 1987;
(b) J. Weidlein, in: Gmelin Handbook of Inorganic Chemistry, Indium, Organoindium Compounds. Part 1. Springer, Berlin, New York, 1991.
[8] P. Fleurat-Lessard, F. Volatron, Inorg. Chem. 39 (2000) 1849.
[9] C. von Hänisch, O. Hampe, Angew. Chem. Int. Ed. Engl. 41 (2002) 2095.
[10] A.F. Wells, Structural Inorganic Chemistry, fifth ed., Oxford Science Publications, Oxford, 1984.
[11] A.H. Cowley, R.A. Jones, M.A. Mardones, J.L. Atwood, S.G. Bott, Angew. Chem. Int. Ed. Engl. 29 (1990) 1409.
[12] M. Driess, S. Kuntz, K. Merz, H. Pritzkow, Chem. Eur. J. 4 (1998) 1628.
[13] C. von Hänisch, F. Weigend, Z. Anorg. Allg. Chem. 628 (2002) 389.
[14] M. Driess, S. Kuntz, C. Monsé, K. Merz, Chem. Eur. J. 6 (2000) 4343.
[15] (a) M. Driess, K. Merz, H. Pritzkow, R. Janoschek, Angew. Chem. Int. Ed. Engl. 35 (1996) 2507;
(b) J.A.L. Cooke, A.P. Purdy, R.L. Wells, P.S. White, Organometallics 15 (1996) 84;
(c) R.J. Wehmschulte, P.P. Power, J. Am. Chem. Soc. 118 (1996) 791.
[16] R.E. Allen, M.A. Beswick, P.R. Raithby, A. Steiner, D.S. Wright, J. Chem. Soc., Dalton Trans., 1996, 4153.
[17] C. Dohmeier, H. Schnöckel, C. Robl, U. Schneider, R. Ahlrichs, Angew. Chem. Int. Ed. Engl. 33 (1994) 199.
[18] C.K.F. von Hänisch, C. Üffing, M.A. Junker, A. Ecker, B.O. Kneisel, H. Schnöckel, Angew. Chem. Int. Ed. 35 (1996) 2875.
[19] W. Köstler, G. Linti, Eur. J. Inorg. Chem. (2001) 1841.
[20] F. Gahlmann, B. Neumüller, Angew. Chem. Int. Ed. Engl. 32 (1993) 1701.
[21] S. Chitsaz, B. Neumüller, Z. Anorg. Allg. Chem. 627 (2001) 2451.
[22] W. Uhl, Z. Naturforsch. 43b (1988) 1113.
[23] C. Dohmeier, C. Robl, M. Tacke, H. Schnöckel, Angew. Chem. Int. Ed. Engl. 30 (1991) 564.
[24] M.A. Petrie, P.P. Power, Organometallics 12 (1993) 1592.
[25] K. Niediek, B. Neumüller, Chem. Ber. 127 (1994) 67, and references cited therein.
[26] K. Niediek, B. Neumüller, Z. Anorg. Allg. Chem. 621 (1995) 889.
[27] B. Werner, B. Neumüller, Organometallics 15 (1996) 4258.
[28] E. Leiner, M. Scheer, Organometallics 21 (2002) 4448.
[29] W. Uhl, W. Hiller, M. Layh, W. Schwarz, Angew. Chem. Int. Ed. Engl. 31 (1992) 1364.
[30] W. Uhl, M. Benter, Chem. Commun. (1999) 771 and references cited therein.
[31] K.M. Waggoner, S. Parkin, D.C. Pestana, H. Hope, P.P. Power, J. Am. Chem. Soc. 113 (1991) 3597.
[32] R.L. Wells, A. Prudy, A.T. McPhail, C.G. Pitt, J. Chem. Soc., Chem. Commun. (1986) 487.
[33] A. Dashti-Mommertz, B. Neumüller, Z. Anorg. Allg. Chem. 625 (1999) 954.
[34] D.E. Heaton, R.A. Jones, K.B. Kidd, A.H. Cowley, C.M. Nunn, Polyhedron 7 (1988) 1901.
[35] D.A. Atwood, A.H. Cowley, P.R. Harris, R.A. Jones, S.U. Koschmieder, C.M. Nunn, J. Organomet. Chem. 449 (1993) 61.
[36] D.A. Atwood, A.H. Cowley, R.A. Jones, M.A. Mardones, J. Organomet. Chem. 449 (1993) C1.
[37] C. von Hänisch, B. Rolli, Z. Anorg. Allg. Chem. 628 (2002) 2255.

[38] C. von Hänisch, D. Fenske, M. Kattannek, R. Ahlrichs, Angew. Chem. Int. Ed. 38 (1999) 2736.
[39] U. App, K. Merzweiler, Z. Anorg. Allg. Chem. 621 (1995) 1731.
[40] E. Iravani, A. Dashti-Mommertz, B. Neumüller, Z. Anorg. Allg. Chem. 629 (2003) 1136.
[41] S. Chitsaz, T. Breyhan, J. Pauls, B. Neumüller, Z. Anorg. Allg. Chem. 628 (2002) 956.
[42] G. Fritz, Angew. Chem. Int Ed. Engl. 26 (1987) 1111, and references cited therein.